UMERC+METS
2024 Conference

7-9 August | Duluth, MN, USA

A Robust Optimal Control for Docking and Charging Unmanned Underwater Vehicles Powered by Wave Energy

Abishek Subramanian[a], Kai Zhou[b], Shangyan Zou[a,*]

[a]*Department of Mechanical Engineering – Engineering Mechanics, Michigan Technological University, 1400 Townsend Dr, Houghton, MI 49931, USA*

[b]*Department of Civil and Environmental Engineering, Hong Kong Polytechnic University, 11 Yuk Choi Rd, Hung Hom, Hong Kong, China*

Abstract

This paper introduces a simulation framework and a corresponding Robust Optimal Control (ROC) for docking Unmanned Underwater Vehicles (UUVs) that leverages Marine Renewable Energy (MRE) for improved autonomy in docking and charging operations. The proposed simulation framework integrates the dynamics of the Wave Energy Converter (WEC), docking station, and UUV within a unified system. Utilizing the WEC-Sim for the hydrodynamic modeling and MoorDyn for mooring dynamics, and in-house UUV dynamics in Simulink, the simulation effectively accounts for complex interactions under dynamic ocean conditions. The ROC docking controller, consisting of a Linear Quadratic Regulator (LQR) and a Sliding Mode Control (SMC), is designed to enhance robustness against environmental disturbances and system uncertainties. This controller utilizes input-output linearization to transform the nonlinear dynamics into a manageable linear form, optimizing docking performance while compensating for disturbances and uncertainties. The combined simulation and control approach is validated under various ocean conditions, demonstrating effective docking precision and energy efficiency. This work lays a foundational platform for future advancements in autonomous marine operations for UUV docking systems integrated with WEC. In addition, this work also demonstrates the feasibility of using MRE to significantly extend the operational duration of UUVs; such a platform will be leveraged for further development of structural health monitoring and fault diagnosis techniques for offshore structures such as WECs and Floating Offshore Wind Turbines.

Keywords: Robust Optimal Controller, UUV-WEC simulation framework, Docking Trajectory Tracking

1. Introduction

In recent years, UUVs have been increasingly used to replace human operators to conduct dangerous and remote missions such as ocean mapping, offshore structure health monitoring, fault diagnosis, and maintenance, detecting and clearing mines, long-range reconnaissance, maritime security, water sample collection, lost equipment recovery, and so forth [1-3]. Despite their advantages, UUVs encounter significant operational challenges, including the need for manual retrieval, recharging, and redeployment. These processes not only introduce substantial costs but also pose

* Corresponding author
E-mail address: shangyan@mtu.edu

considerable risks and safety concerns [4]. Utilizing Marine Renewable Energy (MRE) from environmental sources, especially wave power (abundant, consistent, and high-power density [5]), offers a new solution [6]. These MRE-powered docking and charging stations could continuously harvest wave power, typically paired with energy storage units such as battery banks, to enable on-demand, at-sea, and autonomous recharging and surface communication for UUV [7]. Despite the promising opportunity presented, the investigation of using wave power for UUVs charging is still at an early stage. On the one hand, the docking and charging technology are still under development by the U.S. military and its industrial partners [8]. On the other hand, the autonomous control of UUV coupled with WEC system is also insufficiently studied [9]. Significant knowledge gaps are holding back the improved autonomy of UUVs that take advantage of wave-powered recharging capabilities. More specifically: (1) there is a lack of an accurate and efficient integrated simulation framework to describe WEC-UUV behavior; (2) there is a lack of UUV control that is optimal, robust, and adaptive, subject to the highly nonlinear dynamics and uncertain ocean environment. Therefore, in this paper, to address these challenges, we will (1) develop a detailed simulation framework that integrates the WEC, docking station, and UUV, which can simulate the UUV docking and charging performance efficiently and accurately; (2) develop a robust optimal control to optimize the UUV docking performance subject to dynamic ocean environments and uncertainties; (3) validate the control performance in varied ocean conditions.

As far as hydrodynamics is concerned, a wide variety of models exist for WECs, ranging from linear models to fully nonlinear CFD-based models [10]. Among these, the linear hydrodynamic model is widely applied in control development and in predicting the dynamic responses of WECs [11-13]. Although higher fidelity models, such as nonlinear potential flow or CFD-based models, can provide better accuracy, their high computational cost limits their applications (particularly in control development and system design). In fact, the linear model is considered as the most optimal approach to balance accuracy and efficiency [14], which is well-suited to be applied in the proposed simulation framework that considers the WEC-Dock-UUV as a whole. Although some highly nonlinear physical phenomena, such as wave breaking and turbulence, are not well captured by linear models, these models can incorporate nonlinear terms resulting from mooring forces, viscous drag, and PTO forces [15]. This significantly improves accuracy, especially when considering the complete WEC system from wave to wire. In this context, a linear wave theory-based hydrodynamic simulator, WEC-Sim, is thus applied in the proposed simulation framework to predict the dynamic behavior of both the WEC and the docking station. It is noted that the mooring forces will be simulated by MoorDyn which is a lumped-mass mooring model that is coupled with WEC-Sim. Further, the subsea docking station is assumed to be connected with the WEC via a cable and is modeled as a non-hydro body (while considering the viscous drag, hydrostatic, and cable reaction forces), given that it is deeply submerged which represents negligible hydrodynamics. With regard to the UUV, BlueROV2 is applied in this research as the case study, given that it is affordable, widely popular, and combines open-source software and hardware which allows fast development, modification, and improvements. Recently, a dynamic model of BlueROV2 has been proposed in [16] (rigid body dynamics subject to viscous drag and added mass) with model parameters calibrated via experimental tests, which is adopted in the simulation framework.

Mobile docking stations although are expected to significantly improve the mission duration and automation of UUVs, it naturally poses challenges for UUV control especially when the docking station/WEC experiences energetic ocean waves and currents. The development of control algorithms relies on the understanding of the dynamics of WEC-dock system subject to varying ocean environments. However, to date, the study of the coordination and autonomous control of UUVs for underwater docking with wave-powered docking stations is very limited. Study [17] proposed a hybrid docking approach which is composed of a path planner and two guidance laws which enables an underactuated UUV to reach the docking station with a heading that is parallel to its entrance in the presence of cross currents. The two guidance laws include an Integral Line of Sight (ILOS) guidance and a Speed Regulated Guidance (SRG) which is used to follow a straight in the phase of approach and adjust the docking angle when the vehicle is in close proximity. However, the docking station considered in this study is static and only ocean current effect is considered. Study [9] proposed a finite horizon Model Predictive Control (MPC) for the UUV to demonstrate the feasibility of rendezvous-style docking (achieved through zero relative position and velocity), wherein the WEC is assumed to undergo ideal sinusoidal motion. This pioneering work successfully showed the viability of the proposed concept, albeit in a highly idealized scenario (e.g., lacking a detailed WEC model). Recently, study [18,19] proposed the integration of a flow state estimator into the design of MPC aims at estimating unknown disturbances under varied ocean current conditions and adjusting docking maneuver correspondingly.

It is worth noting that in order to accomplish the final attachment to the target in the proposed docking problem, the UUV needs to not only approach to but also synchronize with it, which is challenging especially considering the docking station is uncontrollable and the disturbances and uncertainties arise from the complex interaction between

the dynamic ocean environment and the system. Therefore, in this paper, we propose a robust control for docking with the uncontrolled target subject to uncertainties and disturbances. More specifically, the nonlinear relative motion dynamics (in which the docking station motion is considered as a reference signal and assumed to be available) is first linearized by using an input-output linearization technique (with disturbances and uncertainties) such that transforming the original nonlinear problem to a linear one with fully decoupled inputs and outputs, so that linear control strategies can be applied. In this scenario, we developed a Linear Quadratic Regulator (LQR) optimal control to optimize the docking performance (e.g., minimize the docking time and fuel consumption). Moreover, to compensate for the disturbances and uncertainties in the system, a Sliding Mode Control (SMC) is also developed in addition to the LQR such that the resulting Robust Optimal Control (ROC) is both optimal and robust. It is noted that to further improve the robustness of the SMC, the sliding surface is designed in an integral manner.

The rest of the paper is organized as follows. Section 2 introduces the proposed integrated simulation framework which includes the WEC, docking station, and the UUV. The mathematical derivations of the ROC are presented in Section 3. Numerical simulation results are presented in Section 4 which compares the performance of ROC to LQR, with discussions of the results and current limitations. Finally, the conclusion is drawn in Section 5.

2. Numerical Modelling

This section introduces the proposed WEC-UUV simulation framework which is composed of three main parts (1) WEC/docking station hydrodynamics and mooring dynamics simulated by using WEC-Sim; (2) In-house UUV dynamics package developed in Simulink; (3) WEC-UUV docking control module developed in Simulink. The complete simulation framework is developed in MATLAB/Simulink and the proposed WEC-UUV docking configuration is presented in Fig. 1.

2.1. WEC and Dock model

The hydrodynamics of the WEC can be expressed by using the Cummins equation [20]:

$$(\boldsymbol{M}_r + \boldsymbol{M}_\infty)\ddot{\vec{x}} = \vec{F}_e + \vec{F}_{PTO} + \vec{F}_r + \vec{F}_s + \vec{F}_m + \vec{F}_v + \vec{F}_c \tag{1}$$

where $\vec{x} = [x, y, z, \phi, \theta, \psi]$ is the state vector which represents the 6 degrees of freedom (DoF) displacement (surge, sway, heave, roll, pitch, yaw) expressed in the body-fixed frame. The matrix M_r is the rigid body mass and matrix M_∞ is the added mass at infinite frequency. Moreover, $\vec{F}_{PTO}$ represents the Power Take-Off (PTO) force, $\vec{F}_m$ denotes the mooring force vector which is calculated by MoorDyn in WEC-Sim which applies a lumped-mass based finite element model to model the mooring dynamics, and $\vec{F}_s$ denotes the linear hydrostatic restoring force. Further, $\vec{F}_r$ represents the radiation force vector which can be expressed by a convolutional integral to account for the fluid memory effect:

$$\vec{F}_r = -\boldsymbol{M}_\infty \ddot{\vec{x}} - \int_0^t \boldsymbol{K}_r(t-\tau)\dot{\vec{x}}(\tau)d\tau \tag{2}$$

In this equation $\boldsymbol{K}_r$ is the radiation impulse response function matrix which can be obtained from the radiation damping and added mass calculated from Boundary Element Method (BEM) software such as WAMIT [21]. The excitation force subject to irregular ocean waves can be computed as the summation of regular wave components:

$$\vec{F}_e = \Re[R_f(t)\sum_{i=1}^{N} \vec{\bar{F}}_e(\omega_i)\eta(\omega_i)e^{i(\omega_i t + \phi_i)}] \tag{3}$$

where $R_f(t)$ is the ramp function, ω_i and ϕ_i denotes the wave frequency and random phase shift of the ith ocean wave. Moreover, $\eta(\omega)$ denotes the frequency-dependent wave elevation which can be computed from specific wave spectrums and $\vec{\bar{F}}_e(\omega)$ is the complex excitation force coefficient which can also be obtained from BEM software WAMIT. Quadratic drag is applied in WEC dynamics:

$$\vec{F}_v = -C_D\dot{\vec{x}}|\dot{\vec{x}}| \tag{4}$$

where C_D is the quadratic drag coefficient. Finally, $\vec{F}_c$ denotes the cable force vector, which is composed of a quadratic drag component and a discontinuous part that applies linear damping and stiffness only when the cable is stretched:

$$\vec{F}_{c,d} = \begin{cases} \vec{0}, & L < L_0 \\ -K_c(\vec{x}_F - \vec{x}_B) - C_c(\dot{\vec{x}}_F - \dot{\vec{x}}_B), & L \geq L_0 \end{cases} \tag{5}$$

In this equation, K_c and C_c represent the damping and stiffness coefficients, respectively, and $\vec{x}_F$ and $\vec{x}_B$ denote the position of the follower and base (which are the docking station and the WEC), respectively.

As far as the docking station is concerned, it is modelled as a drag body in WEC-Sim. More specifically, the hydrostatic force, cable reaction forces, and quadratic drag force are considered in simulating the dynamic behavior of the docking station. The hydrodynamic forces are neglected given that they are deeply submerged in the water.
In this study, a generic point absorber WEC, Reference Model 3 (RM3), is used as the representative WEC [22]. The configuration of RM3 is presented in Fig. 1. The device consists of two bodies: a floating body and a spar-plate. The relative motion between the two bodies, driven by the ocean waves, will be utilized to generate useful electricity. It is noted that in research, a passive PTO is applied for wave power production. Developing more sophisticated PTO control is beyond the scope of this paper, and interested readers can refer to [23-25]. Additionally, three mooring lines are connected to the WEC to maintain its position, which are composed of upper lines (between the WEC and point masses) and lower lines (between point masses and the seabed). The key parameters of RM3 are presented in Table 1. Moreover, the docking station is also presented in Fig. 1, which has a box shape with a total height of 1.5m. It is connected to the bottom of the spar-plate of RM3 via a cable with an unstretched length of 20m. The key parameters of the docking station and the cable are summarized in Table 2a and Table 2b respectively.

Table 1: RM3 key parameters

RM3 Float		**RM3 Spar**		**PTO and Mooring**	
Mass (kg)	749110	Mass (kg)	876420	PTO damping (Ns/m)	1.2 $\times 10^6$
Moment of Inertia (x) (kg.m^2)	20907301	Moment of Inertia (x) (kg.m^2)	94419614.57	Mooring material density (kg/m^3)	7736.7
Moment of Inertia (y) (kg.m^2)	21306090.66	Moment of Inertia (y) (kg.m^2)	94407091.24	Mooring line diameter (m)	0.144
Moment of Inertia (z) (kg.m^2)	37085481.11	Moment of Inertia (z) (kg.m^2)	28542224.82		
Quadratic Drag Coefficient (Cd)	[1, 1, 1]	Quadratic Drag Coefficient (Cd)	[3.5,3.5,3.5]		
Center of Gravity (m) in global frame	[0, 0, -0.72]	Center of Gravity (m) in global frame	[0, 0, -21.29]		

Table 2: Docking station and cable key parameters

Docking Station		**Suspending cable**	
Mass (kg)	2228.17	Stiffness (N/m)	1000000
Volume (m^3)	0.825	Damping (Ns/m)	100
Moment of Inertia (x) (kg.m^2)	1185.218	Quadratic Drag Coefficient (Cd)	[1.4, 1.4, 1.4]
Moment of Inertia (y) (kg.m^2)	1356.937	Cable top in global frame (m)	[0, 0, -30]
Moment of Inertia (z) (kg.m^2)	1185.218	Cable bottom in global frame (m)	[0, 0, -49.25]
Quadratic Drag Coefficient (Cd)	[1.2,1.2,1.2]		
Center of Gravity (m) in global frame	[0, 0, -50]		

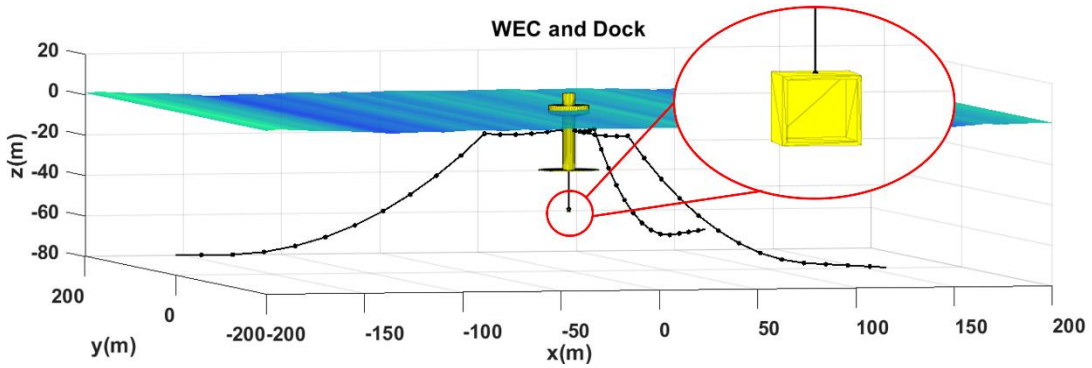

Figure 1: Layout of the proposed WEC-UUV simulation framework.

2.2. UUV Dynamics

In this research, the BlueUUV2 is applied as the representative UUV (as presented in Fig. 2). The dynamics of this UUV is developed and calibrated by experimental data in a recent publication [13] which will also be adopted in this paper and be briefly introduced in the following. The dynamics is expressed in a $\vec{\eta} - \vec{v}$ Fossen notation as:

$$\dot{\vec{\eta}} = \boldsymbol{J}(\vec{\eta})\vec{v}$$
$$\boldsymbol{M}\dot{\vec{v}} + \boldsymbol{C}(\vec{v}) + \boldsymbol{D}(\vec{v})\vec{v} + \boldsymbol{g}(\vec{\eta}) = \vec{\tau} \quad (6)$$

where $\vec{\eta} = [x, y, z, \phi, \theta, \psi]^T$ represents the 6 DoF position of the UUV in the global frame (which is assumed to be North-East-Down (NED)) and $\vec{v} = [u, v, w, p, q, r]^T$ denotes the velocity of the vehicle expressed in the body-fixed frame. Further, the matrix $\boldsymbol{M} = \boldsymbol{M}_{RB} + \boldsymbol{M}_A$ is a constant, symmetric and strictly positive definite inertia matrix combining the rigid-body inertia matrix $\boldsymbol{M}_{RB}$ and the added-mass inertia matrix $\boldsymbol{M}_A$. The matrix $\boldsymbol{C}(\vec{v}) = \boldsymbol{C}_{RB}(\vec{v}) + \boldsymbol{C}_A(\vec{v})$ is a skew-symmetric Coriolis matrix combining the rigid-body Coriolis-centripetal matrix C_{RB} and added-mass Coriolis-centripetal matrix $\boldsymbol{C}_A$. The matrix $\boldsymbol{D}(\vec{v}) = \boldsymbol{D} + \boldsymbol{D}_n(\vec{v})$ is the hydrodynamic damping matrix combining the diagonal matrix $\boldsymbol{D}$ containing the linear damping coefficients and the diagonal matrix $\boldsymbol{D}_n$ containing the quadratic damping coefficients. The matrix $\boldsymbol{g}(\vec{\eta})$ contains the vector of restoring forces (gravitational and buoyancy forces) acting along all the six degrees of freedom at the origin of the b-frame which is taken as the center of mass of the vehicle. The detailed elements of each matrix can be found in [13] and will not be redundant in this paper. Finally, $\vec{\tau}$ represents the thrust force of the UUV, which is the control force; the details of its design are provided in the next section.

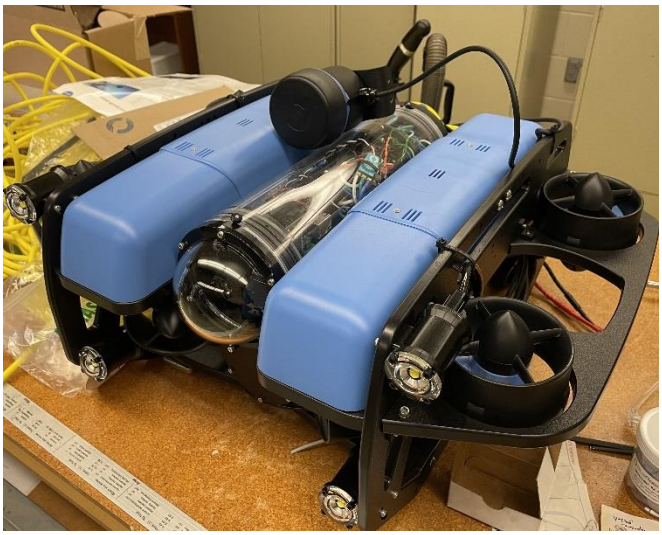

Figure 2: BlueRov2 hardware configuration.

3. Robust Optimal Control development

This section will introduce the development of the ROC with detailed mathematical derivations. The control is composed of an LQR for optimizing the docking performance and an SMC to regulate disturbances and uncertainties. Moreover, an input-output linearization technique is also applied to transform the original system so that linear optimal controls can be applied.

3.1. Control problem statement and input-output linearization.

The objective of the control is to drive the UUV dock with the docking station in an optimal manner subject to uncertainties and disturbances. In this context, we first formulate the error vector as:

$$\vec{e} = \vec{\eta} - \vec{x} \quad (7)$$

where $\vec{\eta}$ and $\vec{x}$ denote the position of the UUV and the position of the docking station respectively. It is noted that the WEC/Dock system is an uncontrollable target, and we assume the trajectory of the docking station (and its derivations such as velocity and acceleration) is measurable and can be communicated with the UUV. Therefore, in the control problem, the motion of the docking station is considered as a reference signal. Moreover, in formulating the control problem, we will take uncertainties and disturbances into consideration (in addition to the nominal dynamics presented in Eq (1) for the WEC and Eq (6) for the UUV). Given that the motion of the docking station is directly measured which reflects the uncertainties and disturbances to some extent, we will mainly consider the uncertainties in UUV dynamics which can be formulated when the UUV dynamics is expressed in a state-space format:

$$\dot{\vec{x}}_1 = \boldsymbol{J}(\vec{x}_1)\vec{x}_2$$
$$\dot{\vec{x}}_2 = -\boldsymbol{M}^{-1}\big(\boldsymbol{C}(\vec{x}_2) + \boldsymbol{D}(\vec{x}_2)\vec{x}_2 + \boldsymbol{g}(\vec{x}_1)\big) + \Delta f(\vec{x}_1, \vec{x}_2) + \boldsymbol{M}^{-1}(\vec{\tau} + \delta(t, \vec{x}_1, \vec{x}_2, \vec{\tau})) \quad (8)$$

where the states $\vec{x}_1 = \vec{\eta}$ and $\vec{x}_2 = \vec{v}$. Furthermore, $\Delta f(\vec{x}_1, \vec{x}_2)$ and $\delta(t, \vec{x}_1, \vec{x}_2, \vec{\tau})$ represent system uncertainties and disturbances including unmodelled dynamics, parameter variations, and external disturbances. To formulate the tracking problem, we are interested in knowing the position vector of the UUV (e.g., Eq. (7) the tracking error), so the output is expressed as:

$$\vec{y} = \vec{x}_1 \tag{9}$$

One can tell from Eq (8) that it is difficult to design a linear control according to Eq. (8) to minimize the tracking error. Therefore, an input-output linearization technique will be presented to linearize the UUV dynamics such that linear optimal controls can be applied. We will first perform the nonlinear state transformation (instead of defining states as $\vec{x}_1$ and $\vec{x}_2$) which requires the continuous differentiation of the system output under the control shows up:

$$\begin{aligned}
\dot{\vec{y}} &= \boldsymbol{J}(\vec{x}_1)\vec{x}_2 \\
\ddot{\vec{y}} &= \frac{d}{dt}\left(\boldsymbol{J}(\vec{x}_1)\vec{x}_2\right) \\
&= \frac{\partial(\boldsymbol{J}(\vec{x}_1)\vec{x}_2)}{\partial\,\vec{x}_1}\dot{\vec{x}}_1 + \frac{\partial(\boldsymbol{J}(\vec{x}_1)\vec{x}_2)}{\partial\vec{x}_2}\dot{\vec{x}}_2 \\
&= \left(\frac{\partial \boldsymbol{J}(\vec{x}_1)}{\partial\vec{x}_1}(\vec{x}_2 \otimes I_n) + \boldsymbol{J}(\vec{x}_1)\frac{\partial\vec{x}_2}{\partial\vec{x}_1}\right)\boldsymbol{J}(\vec{x}_1)\vec{x}_2 \\
&\qquad + \left(\frac{\partial \boldsymbol{J}(\vec{x}_1)}{\partial\vec{x}_2}(\vec{x}_2 \otimes I_n) + \boldsymbol{J}(\vec{x}_1)\frac{\partial\vec{x}_2}{\partial\vec{x}_2}\right)\Big(-\boldsymbol{M}^{-1}\big(\boldsymbol{C}(\vec{x}_2) + \boldsymbol{D}(\vec{x}_2)\vec{x}_2 + \boldsymbol{g}(\vec{x}_1)\big) \\
&\qquad + \Delta f(\vec{x}_1, \vec{x}_2) + \boldsymbol{M}^{-1}\big(\vec{\tau} + \delta(t, \vec{x}_1, \vec{x}_2, \vec{\tau})\big)\Big)
\end{aligned} \tag{10}$$

where $\otimes$ denotes the Kronecker product and n represents the dimension of vector in the dominator of the partial derivative. More details of the partial derivatives of the coordinate transformation matrix subject to the position and velocity vector can be found in the appendix. We will stop the differentiation since the control already appears. This also indicates the relative degree of each decoupled subsystem of this multi-input-multi-output (MIMO) system is two. To simplify the rest of the derivations we denote:

$$\begin{aligned}
\boldsymbol{S}_1 &= \frac{\partial \boldsymbol{J}(\vec{x}_1)}{\partial\vec{x}_1}(\vec{x}_2 \otimes I_n) + \boldsymbol{J}(\vec{x}_1)\frac{\partial\vec{x}_2}{\partial\vec{x}_1} \\
\boldsymbol{S}_2 &= \frac{\partial \boldsymbol{J}(\vec{x}_1)}{\partial\vec{x}_2}(\vec{x}_2 \otimes I_n) + \boldsymbol{J}(\vec{x}_1)\frac{\partial\vec{x}_2}{\partial\vec{x}_2}
\end{aligned} \tag{11}$$

Now, apply the nonlinear state transformation we define $\vec{\zeta}_1 = \vec{y}$ and $\vec{\zeta}_2 = \dot{\vec{y}}$, and we have

$$\begin{aligned}
\dot{\vec{\zeta}}_1 &= \vec{\zeta}_2 \\
\dot{\vec{\zeta}}_2 &= \boldsymbol{S}_1\boldsymbol{J}(\vec{x}_1)\vec{x}_2 + \boldsymbol{S}_2\Big(-\boldsymbol{M}^{-1}\big(\boldsymbol{C}(\vec{x}_2) + \boldsymbol{D}(\vec{x}_2)\vec{x}_2 + \boldsymbol{g}(\vec{x}_1)\big) + \Delta f(\vec{x}_1, \vec{x}_2) \\
&\qquad + \boldsymbol{M}^{-1}\big(\vec{\tau} + \delta(t, \vec{x}_1, \vec{x}_2, \vec{\tau})\big)\Big)
\end{aligned} \tag{12}$$

According to this, we can next define the error states $\vec{e}_1 = \zeta_1 - \vec{x}$ and $\vec{e}_2 = \zeta_2 - \dot{\vec{x}}$, and further express the tracking error dynamics as:

$$\begin{aligned}
\dot{\vec{e}}_1 &= \vec{e}_2 \\
\dot{\vec{e}}_2 &= \boldsymbol{S}_1\boldsymbol{J}(\vec{x}_1)\vec{x}_2 + \boldsymbol{S}_2\Big(-\boldsymbol{M}^{-1}\big(\boldsymbol{C}(\vec{x}_2) + \boldsymbol{D}(\vec{x}_2)\vec{x}_2 + \boldsymbol{g}(\vec{x}_1)\big) + \Delta f(\vec{x}_1, \vec{x}_2) \\
&\qquad + \boldsymbol{M}^{-1}\big(\vec{\tau} + \delta(t, \vec{x}_1, \vec{x}_2, \vec{\tau})\big)\Big) - \ddot{\vec{x}}
\end{aligned} \tag{13}$$

Now choose the control according to input-output linearization law as:

$$\vec{\tau} = (\boldsymbol{S}_2\,\boldsymbol{M}^{-1})^{-1}(-\boldsymbol{S}_1\boldsymbol{J}(\vec{x}_1)\vec{x}_2 + \boldsymbol{S}_2\,\boldsymbol{M}^{-1}\big(\boldsymbol{C}(\vec{x}_2) + \boldsymbol{D}(\vec{x}_2)\vec{x}_2 + \boldsymbol{g}(\vec{x}_1)\big) + \ddot{\vec{x}} + \vec{u}) \tag{14}$$

In this equation, $\vec{u}$ is an equivalent input which will be designed later. The resulting dynamics of the tracking error is:

$$\begin{aligned}
\dot{\vec{e}}_1 &= \vec{e}_2 \\
\dot{\vec{e}}_2 &= \vec{u} + \boldsymbol{S}_2\Delta f(\vec{x}_1, \vec{x}_2) + \boldsymbol{S}_2\,\boldsymbol{M}^{-1}\delta(t, \vec{x}_1, \vec{x}_2, \vec{\tau})
\end{aligned} \tag{15}$$

which can be written in a matrix format as:

$$\dot{\vec{e}} = \boldsymbol{A}\vec{e} + \Delta\boldsymbol{A} + \boldsymbol{B}\vec{u} + \Delta\boldsymbol{\delta} \tag{16}$$

where $\vec{e} = [\vec{e}_1, \vec{e}_2]^T$ and

$$\begin{aligned}
\boldsymbol{A} &= \begin{bmatrix} 0_{6\times6} & I_6 \\ 0_{6\times6} & 0_{6\times6} \end{bmatrix} \text{ and } \boldsymbol{B} = \begin{bmatrix} 0_{6\times6} \\ I_6 \end{bmatrix} \\
\Delta\boldsymbol{A} &= \begin{bmatrix} 0_{6\times1} \\ \boldsymbol{S}_2\Delta f(\vec{x}_1, \vec{x}_2) \end{bmatrix} \text{ and } \Delta\boldsymbol{\delta} = \begin{bmatrix} 0_{6\times1} \\ \boldsymbol{S}_2\,\boldsymbol{M}^{-1}\delta(t, \vec{x}_1, \vec{x}_2, \vec{\tau}) \end{bmatrix}
\end{aligned} \tag{17}$$

The uncertainties $\Delta\boldsymbol{A}$ and $\Delta\boldsymbol{\delta}$ satisfy the matching condition [26]:

$$\Delta\boldsymbol{A} = \boldsymbol{B}\Delta\boldsymbol{a} \text{ and } \Delta\boldsymbol{\delta} = \boldsymbol{B}\Delta\boldsymbol{b} \tag{18}$$

In this equation $\Delta\boldsymbol{a}$ and $\Delta\boldsymbol{b}$ denote unknown continuous function vectors that are bounded by:

Assumption 1: *There exist known constants α and β such that:*

$$\|\Delta\boldsymbol{a}\|_1 \leq \alpha \text{ and } \|\Delta\boldsymbol{b}\|_1 \leq \beta \tag{19}$$

where $\|\cdot\|_1$ represents the 1-norm. The control problem now has been formulated as a tracking problem with linearized dynamics subject to uncertainties and disturbances, we shall next present the design of the ROC.

3.2. Robust Optimal Control development

We will first design the optimal control subject to the nominal error dynamics:

$$\dot{\vec{e}}_n = \boldsymbol{A}\vec{e}_n + \boldsymbol{B}\vec{u}_l \tag{20}$$

To optimize the performance of docking (e.g., minimum time and fuel consumption), we can define a cost function as:

$$J = \frac{1}{2}\int_0^T [\vec{e}_n(t)\boldsymbol{Q}\vec{e}_n(t)^T + \vec{u}_l(t)^T\boldsymbol{R}\vec{u}_l(t)]dt \tag{21}$$

where $\boldsymbol{Q} \in \boldsymbol{R}^{12\times12}$ and $\boldsymbol{R} \in \boldsymbol{R}^{6\times6}$ are symmetric positive semi definite matrix. According to the optimal control theory the solution to the control input is:

$$\vec{u}_l(t) = -\boldsymbol{R}^{-1}\boldsymbol{B}^T\boldsymbol{P}\vec{e}_n(t) \tag{22}$$

The $\boldsymbol{P}$ represent the covariance matrix which is the solution of the algebraic Riccati equation (ARE):

$$\boldsymbol{P}\boldsymbol{A} + \boldsymbol{A}^T\boldsymbol{P} - \boldsymbol{P}\boldsymbol{B}\boldsymbol{R}^{-1}\boldsymbol{B}^T\boldsymbol{P} + \boldsymbol{Q} = 0 \tag{23}$$

Substituting Eq. (22) back into Eq. (20) give us the closed-loop performance of the nominal error:

$$\dot{\vec{e}}_n = (\boldsymbol{A} - \boldsymbol{B}\boldsymbol{R}^{-1}\boldsymbol{B}^T\boldsymbol{P})\vec{e}_n(t) \tag{24}$$

According to the optimal control theory, the resulting system in Eq. (24) will be asymptotically stable which represents the nominal error (physically is the relative position between the docking station and the UUV without uncertainties) will converge to zero in an optimal manner. This optimal tracking performance can be achieved by balancing the penalty on the tracking error and the control effort (say $\boldsymbol{Q}$ and $\boldsymbol{R}$ matrices). Next, we will design a control to enhance the robustness of the nominal system against uncertainties. The sliding surface is designed in an integral manner to maximize the robustness:

$$\vec{s}(t,\vec{e}) = \boldsymbol{G}\vec{e}(t) - \boldsymbol{G}\vec{e}(0) - \boldsymbol{G}\int_0^t (\boldsymbol{A} - \boldsymbol{B}\boldsymbol{R}^{-1}\boldsymbol{B}^T\boldsymbol{P})\vec{e}(\tau)d\tau \tag{25}$$

where $\boldsymbol{G} \in \boldsymbol{R}^{6\times12}$ is a constant matrix which is designed such that $\boldsymbol{G}\boldsymbol{B}$ is nonsingular. We propose the following ROC control law such that the sliding surface is asymptotically stable, and the nominal system can be optimized:

$$\vec{u}(t) = \vec{u}_l(t) + \vec{u}_s(t) \tag{26}$$

where,

$$\begin{aligned}\vec{u}_l(t) &= -\boldsymbol{R}^{-1}\boldsymbol{B}^T\boldsymbol{P}\vec{e}(t)\\ \vec{u}_s(t) &= -(\boldsymbol{G}\boldsymbol{B})^{-1}\gamma\,\mathrm{sign}(\vec{s})\end{aligned} \tag{27}$$

In this equation $\vec{u}_l(t)$ is the continuous part which is used to optimize the performance of the nominal error system, while $\vec{u}_s(t)$ is the discontinuous part which guarantees the full robustness subject to uncertainties and disturbances. We shall now prove the convergence of the sliding surface.

Theorem 1. *Consider the dynamics of the error in Eq. (16) and Assumption 1. Given the sliding surface defined in Eq. (25), we can apply the ROC designed in Eq. (26) such that the system can reach the sliding surface in finite time and maintain on it if $\gamma \geq (\alpha + \beta)\|\boldsymbol{G}\boldsymbol{B}\|$.*

Proof: Define a positive definite Lyapunov candidate function as:

$$V = \frac{1}{2}\vec{s}^T\vec{s} \tag{28}$$

The derivative can be computed as:

$$\begin{aligned}\dot{V} &= \vec{s}^T\dot{\vec{s}}\\ &= \vec{s}^T(\boldsymbol{G}\dot{\vec{e}}(t) - \boldsymbol{G}(\boldsymbol{A} - \boldsymbol{B}\boldsymbol{R}^{-1}\boldsymbol{B}^T\boldsymbol{P})\vec{e}(t))\\ &= \vec{s}^T(\boldsymbol{G}(\boldsymbol{A}\vec{e} + \Delta\boldsymbol{A} + \boldsymbol{B}\vec{u} + \Delta\boldsymbol{\delta}) - \boldsymbol{G}(\boldsymbol{A} - \boldsymbol{B}\boldsymbol{R}^{-1}\boldsymbol{B}^T\boldsymbol{P})\vec{e}(t))\end{aligned} \tag{29}$$

Now plug in the control:

$$\begin{aligned}\dot{V} &= \vec{s}^T\big(\boldsymbol{G}(\,\boldsymbol{A}\vec{e} + \Delta\boldsymbol{A} + \boldsymbol{B}(-\boldsymbol{R}^{-1}\boldsymbol{B}^T\boldsymbol{P}\vec{e}(t) - (\boldsymbol{G}\boldsymbol{B})^{-1}\gamma\,\mathrm{sign}(\vec{s})) + \Delta\boldsymbol{\delta}) \\ &\qquad - \boldsymbol{G}(\boldsymbol{A} - \boldsymbol{B}\boldsymbol{R}^{-1}\boldsymbol{B}^T\boldsymbol{P}\,)\vec{e}(t)\big) \\ &= \vec{s}^T(\boldsymbol{G}\Delta\boldsymbol{A} - \gamma\,\mathrm{sign}(\vec{s}) + \boldsymbol{G}\Delta\boldsymbol{\delta}) \\ &\leq -\gamma\|\vec{s}\|_1 + \vec{s}^T\boldsymbol{G}(\Delta\boldsymbol{A} + \Delta\boldsymbol{\delta}) \\ &\leq -\gamma\|\vec{s}\|_1 + \|\vec{s}^T\boldsymbol{G}(\Delta\boldsymbol{A} + \Delta\boldsymbol{\delta})\|_1 \\ &= -\gamma\|\vec{s}\|_1 + \|\vec{s}^T\boldsymbol{G}\boldsymbol{B}(\Delta\mathbf{a} + \Delta\mathbf{b})\|_1 \\ &\leq -\gamma\|\vec{s}\|_1 + \|\vec{s}\|_1\|\boldsymbol{G}\boldsymbol{B}\|_1(\|\Delta\mathbf{a}\|_1 + \|\Delta\mathbf{b}\|_1) \\ &\leq -\gamma\|\vec{s}\|_1 + \|\vec{s}\|_1\|\boldsymbol{G}\boldsymbol{B}\|_1(\alpha + \beta)\end{aligned} \tag{30}$$

So eventually we have:

$$\dot{V} \leq -(\gamma - (\alpha + \beta)\|\boldsymbol{G}\boldsymbol{B}\|_1)\|\vec{s}\|_1 \tag{31}$$

It is apparent that if:

$$\gamma > (\alpha + \beta)\|\boldsymbol{G}\boldsymbol{B}\|_1 \tag{32}$$

The derivative of the Lyapunov function is negative definite. Therefore, the sliding manifold is asymptotically stable and that completes the proof.

Finally, we need to transform the derived control back into the dynamic system, and the resulting complete ROC control law is:

$$\begin{aligned}\vec{\tau} = (\boldsymbol{S_2}\,\boldsymbol{M}^{-1})^{-1}(&-\boldsymbol{S_1}\boldsymbol{J}(\vec{x}_1)\vec{x}_2 + \boldsymbol{S_2}\,\boldsymbol{M}^{-1}\big(\boldsymbol{C}(\vec{x}_2) + \boldsymbol{D}(\vec{x}_2)\vec{x}_2 + \boldsymbol{g}(\vec{x}_1)\big) + \ddot{\vec{x}} \\ &- \boldsymbol{R}^{-1}\boldsymbol{B}^T\boldsymbol{P}\vec{e}(t) - (\boldsymbol{G}\boldsymbol{B})^{-1}\gamma\,\mathrm{sign}(\vec{s}))\end{aligned} \tag{33}$$

It is noted that to reduce the chattering of the SMC control, the discontinuous function $\mathrm{sign}(\vec{s})$ will be replaced by a smooth function $\tanh(\alpha\vec{s})$ in the implementation and α is the smoothing factor.

4. Results and Discussions

Numerical simulation results are presented in this section, in which we will present the hydrodynamic performance of the WEC/Dock system under varied wave conditions and the docking performance in terms of both optimality and robustness.

4.1. WEC and Dock hydrodynamics

The integrated simulation framework of the WEC and the suspended docking station as presented in Section 2.1 is tested with different wave conditions to first evaluate the wave elevation. To mimic the real-world scenario, we have used four representative sea states adopted from [27]. The significant wave height (Hs) and the peak period (Tp) are summarized in Table 3. Fig. 3 shows the wave elevation for one wave condition.

Table 3: Wave Conditions

Wave Condition	Significant Wave Height (Hs) (m)	Peak Period (Tp) (s)
Case 1	4.33	13.97
Case 2	1.65	8.81
Case 3	1.96	16.42
Case 4	2.19	11.92

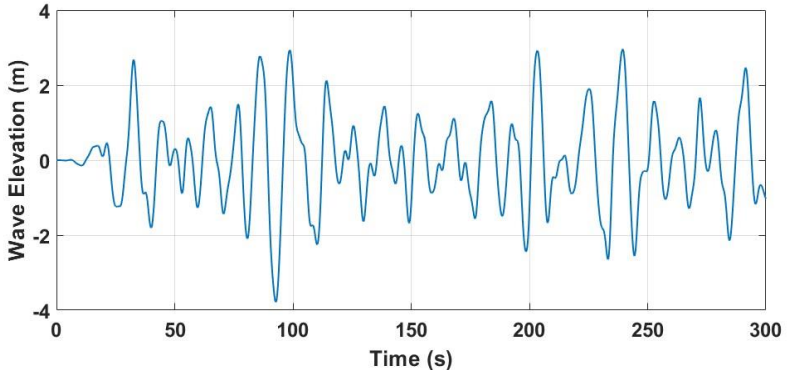

Figure 3: Wave Elevation for Sea State 1 that has a significant wave height of 4.33m and a peak period of 13.97s.

Fig. 4 compares the motion of the float and spar plate of the WEC before and after the addition of the docking station under the most powerful sea state (Case 1 with Hs = 4.33m, Tp = 13.97s). It is noted that all the motion plots are made with respect to the displacement (meaning the initial offset is subtracted) rather than the position. We can tell from the figure that the displacement of the docking station is between [1.73m, -1.98m], [1.02m, -1.75m], and [0.0712rad, -0.773rad] in surge, heave, and pitch, respectively. It is also clearly visible in the figure that the addition of the docking station has a negligible impact on the dynamic response of the WEC. This observation can be further evidenced by the wave power produced by RM3 under four different wave conditions which is summarized in Table 4. The mean wave power productions are nearly the same for the cases with and without the docking station.

Table 4: Mean Power Generation

Wave Condition	**Mean Wave Power Production without Dock (kW)**	**Mean Wave Power Production with Dock (kW)**
Case 1	199.73	199.65
Case 2	46.409	46.411
Case 3	30.565	30.456
Case 4	63.823	63.892

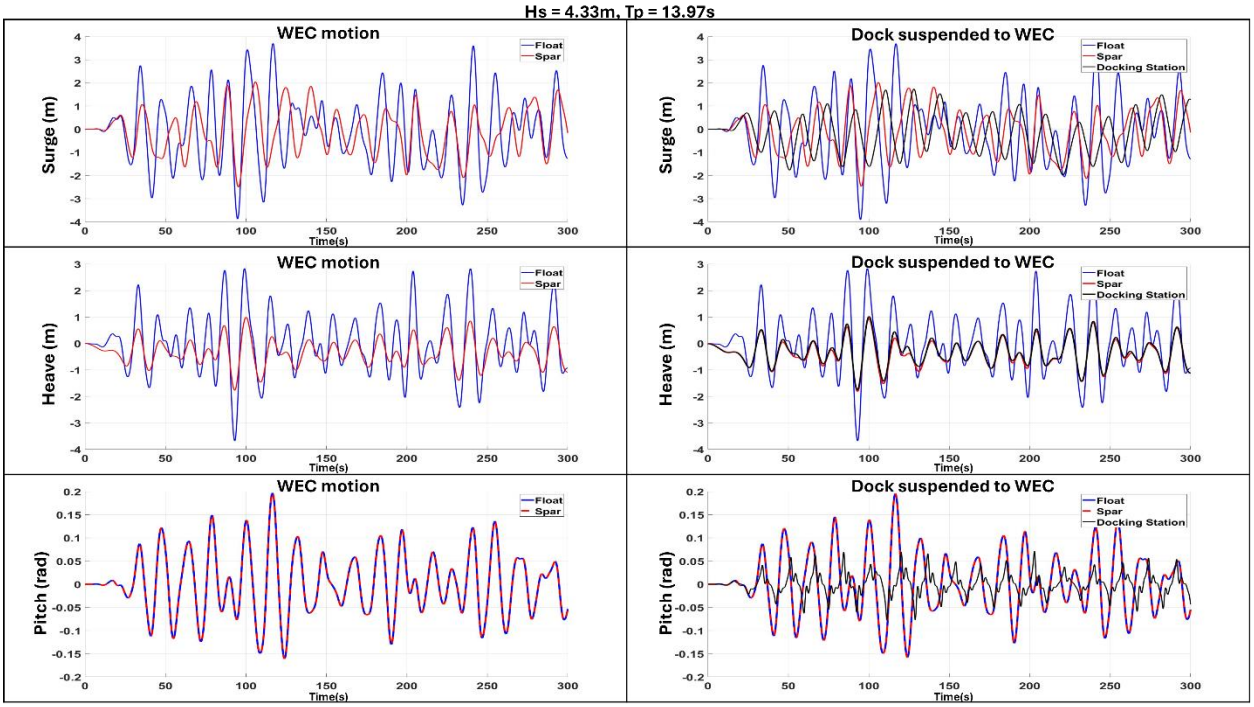

Figure 4: Comparison of WEC and Docking Station motion before and after suspending the docking station

Next, Fig. 5 and 6 further presents the motion of the WEC and the docking station in different sea states. The maximum displacement of the docking station are [0.26m, -0.27m], [1.51m, -1.32m], and [0.59m, -0.83] under sea state 2 (Hs = 1.65m, Tp = 8.91s), sea state 3 (Hs = 1.96m, Tp = 16.42s), and sea state 4 (Hs = 2.19m, Tp = 9.89s), in surge; [0, -0.58], [0.4m, -1.18m], and [0.06m, -0.74] under sea state 2, 3, and 4 in heave; and [0.0189rad, -0.176rad], [0.0641rad, -0.0699rad], and [0.0313rad, -0.0329rad] under sea state 2, 3, and 4 in pitch. In general, the motion of the docking station when it is designed in a mobile manner is significant which requires the control to drive the UUV not only approach the docking station but also synchronize the motion with respect to the dock in a robust manner. Moreover, it is also visible in the figures that the heave motion of the docking station is very close to the heave motion of the spar plate of RM3. This is because the heave dynamic response of the docking station is dominated by the cable tension force and the cable has a relatively large stiffness.

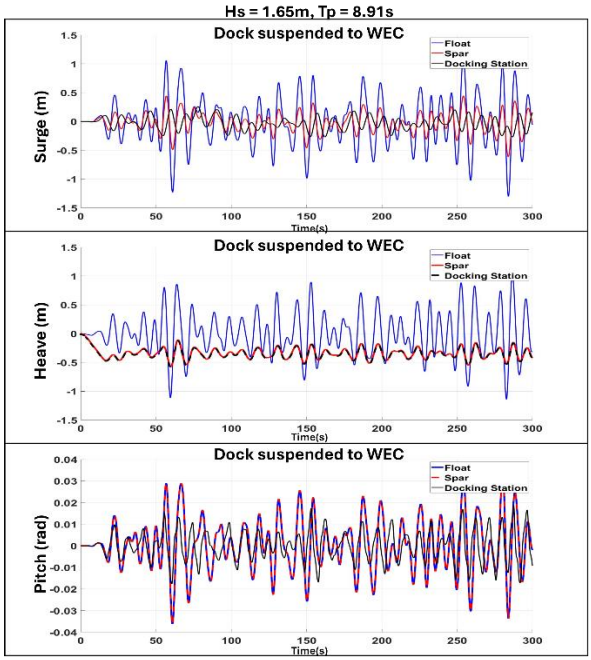

Figure 5: WEC and Docking Station Motion for Case 2

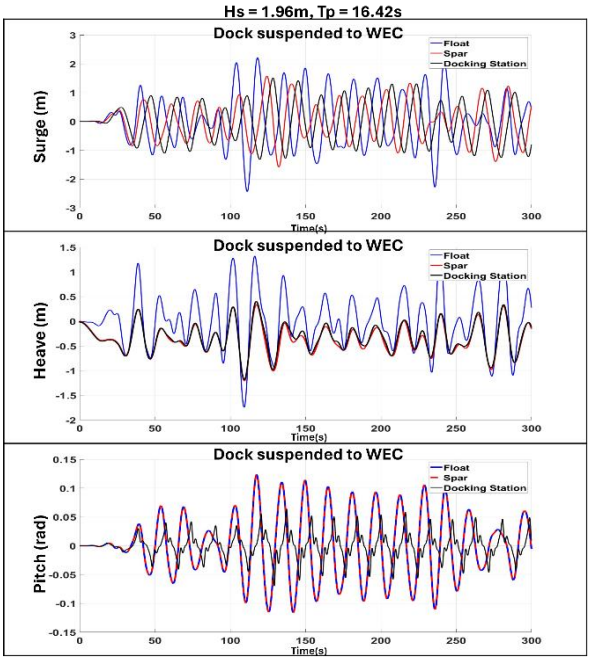

Figure 6: WEC and Docking Station Motion for Case

4.2. Performance of the ROC control

We first consider the ideal scenario where the uncertainties due to unmodelled dynamics and external disturbances are absent, which forms the nominal system, and use the standalone LQR controller to track the trajectory. The wave conditions defined for Case 1 (significant wave height of 4.33m and peak period of 13.97s) presented in Table 4 are used to evaluate the controller's performance henceforth. It is noted that this is the most energetic wave condition which represents a large motion of the docking station. The intention of choosing this wave condition as the case study is to present the control performance subject to a challenging ocean environment. The LQR controller is tuned for optimal performance with: $\mathbf{Q} = \boldsymbol{I}^{12\times12}$ and $\mathbf{R} = 100\boldsymbol{I}^{6\times6}$. It is noted that a relatively high penalty is applied to the control effort to guarantee the resulting control is within the limited thrust force of 85N, 85N, 120N, 26N, 14N, 22N for surge, sway heave, roll, pitch and yaw respectively.

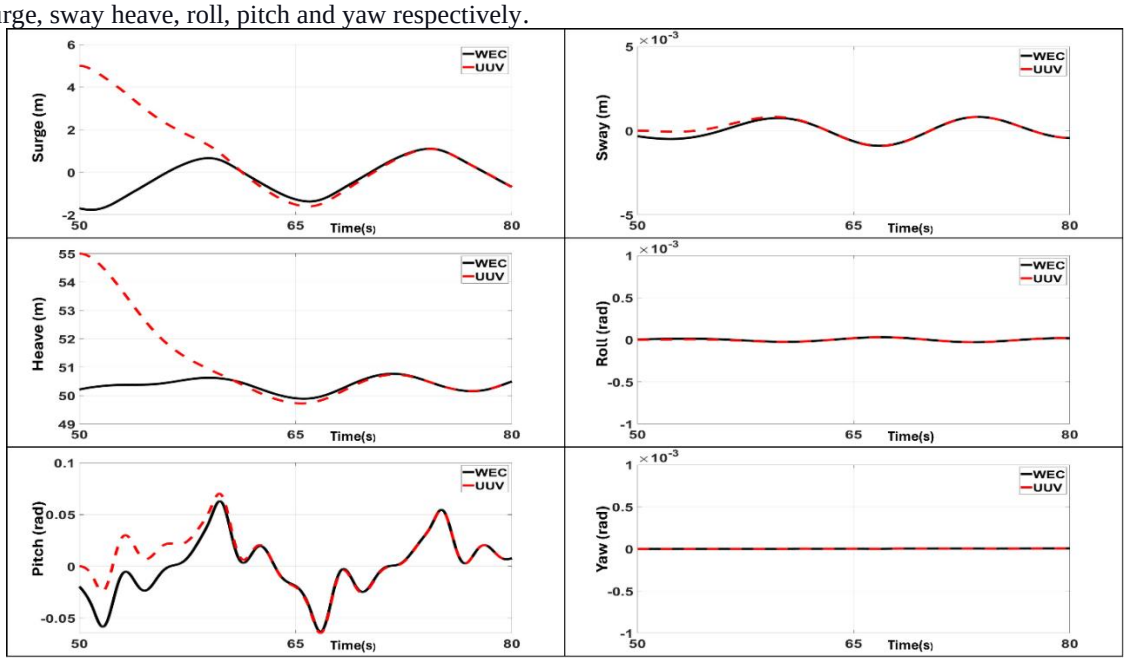

Figure 7: Positional Displacement of WEC and UUV for Ideal Scenario using Standalone LQR Controller

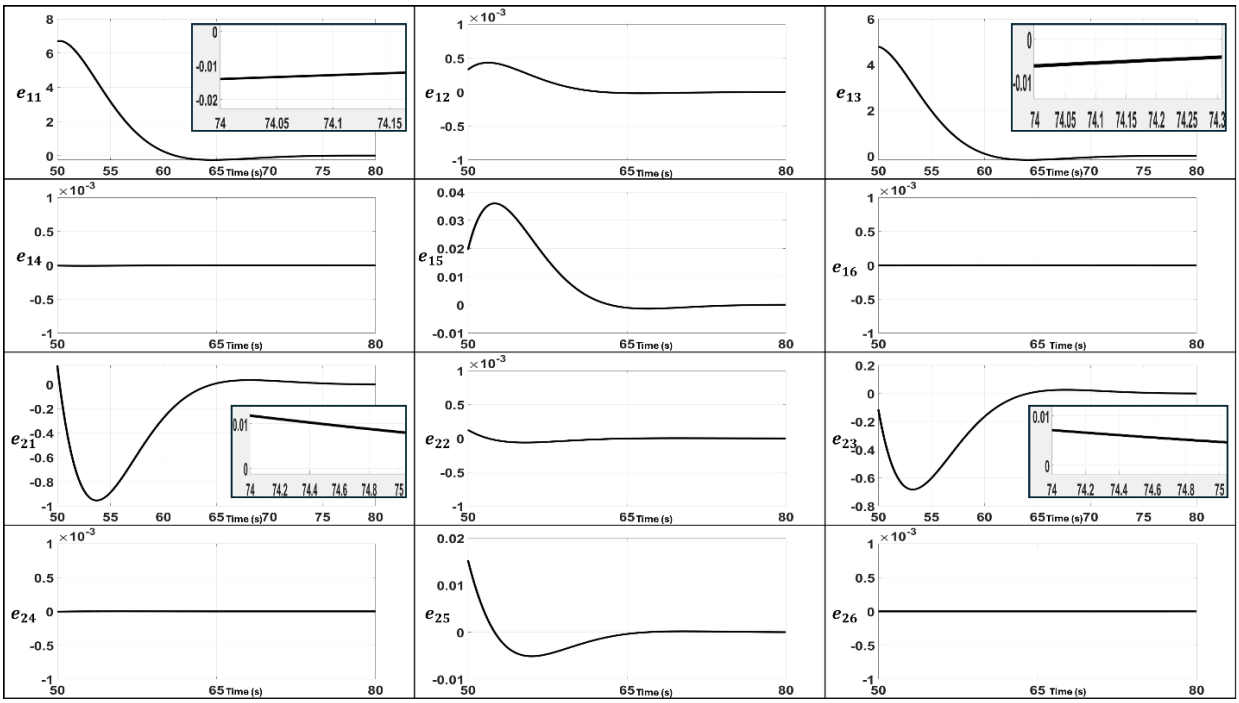

Figure 8: Tracking Error States for Ideal Scenario with Standalone LQR Controller

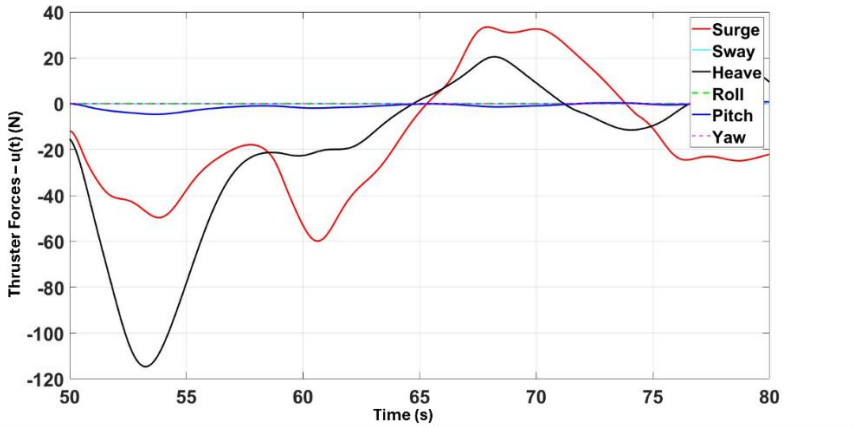

Figure 9: Thruster Actuator Signals for Ideal LQR Controller.

Fig. 7 shows the tracking performance of the UUV with respect to the docking station suspended below the WEC along all six degrees of freedom. Initially, the UUV is positioned at [5, 0, 55, 0, 0, 0] m. We can see that the UUV can successfully track the motion of the WEC, and the docking time is observed to be 24s. More details of the tracking performance are shown in Fig. 8 which presents the tracking error (between the UUV and the docking station) in terms of both the displacement $[\mathrm{e11\ e12, e13, e14, e15, e16}]^T$ and the velocity $[\mathrm{e21\ e22, e23, e24, e25, e26}]^T$. We can tell from the figure that all the tracking errors converge to zero in a finite time. The resulting thruster forces (transformed back from the input-output linearization) of the LQR control is presented in Fig. 9. It is visible in the figure that the thruster forces along all six DOFs are within the upper limit of the actuation forces the thrusters in BlueRov2 can deliver. The total energy the UUV consumes to dock is around 650.1 Joules.

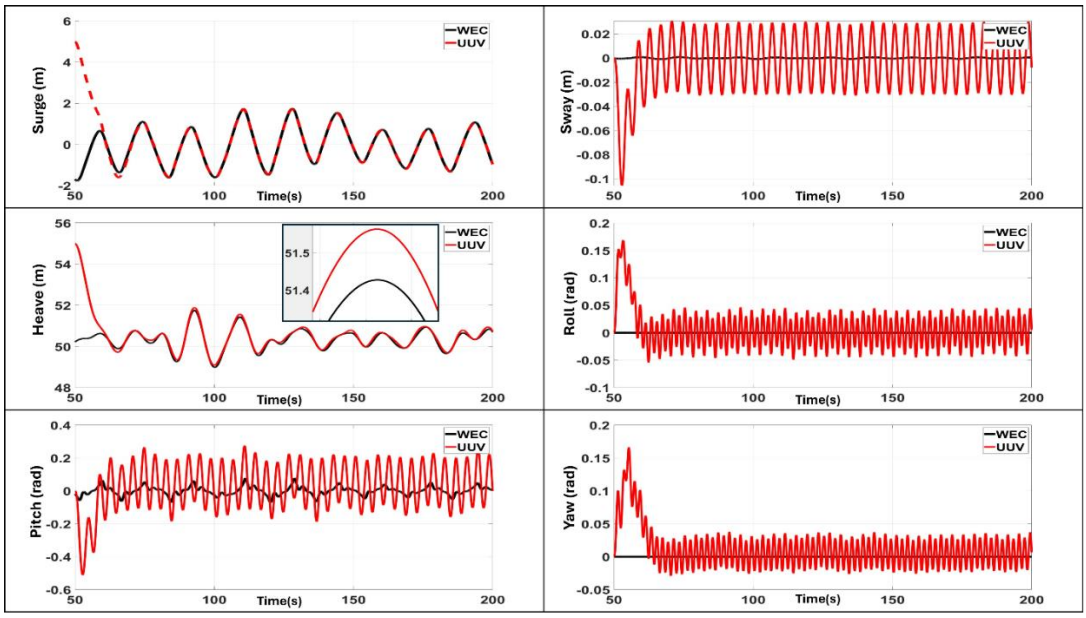

Figure 10: Positional Displacement of WEC and UUV for Actual Scenario using Ideal LOR Controller.

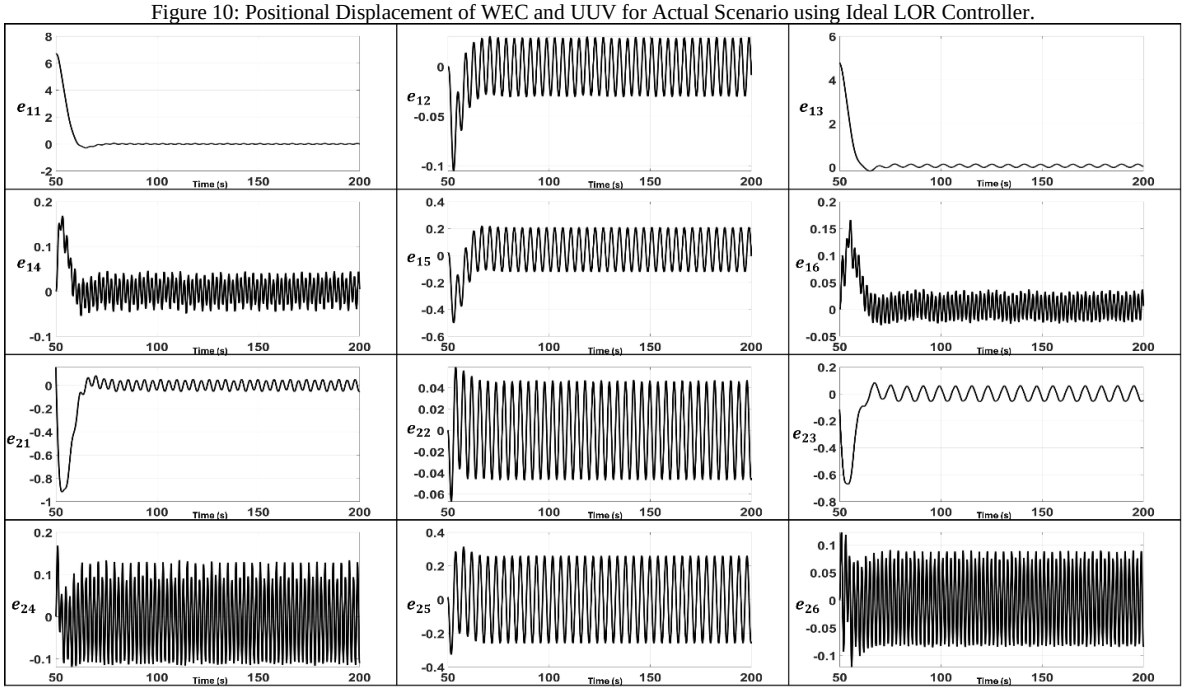

Figure 11: Tracking Error States for Actual Scenario using Ideal LOR Controller

Next, we consider the actual scenario with uncertainties from unmodelled dynamics and external disturbances. We represent the uncertainties using sin waves with an amplitude of 1.5m in surge, sway and heave motion and an amplitude of 0.15 rad in roll, pitch and yaw motion. The initial position of the UUV is the same as in the previous scenario. Fig. 10 shows the tracking performance of the standard LQR controller in the actual scenario with uncertainties. We can see that the UUV cannot track the docking station and the tracking errors presented in Fig. 11 cannot converge to zero. There is a significant deviation in the trajectory along all six DOFs as well as the relatively velocity between the UUV and the docking station. This is expected since the LQR control can only optimize the nominal system without the capability to handle uncertainties and disturbances.

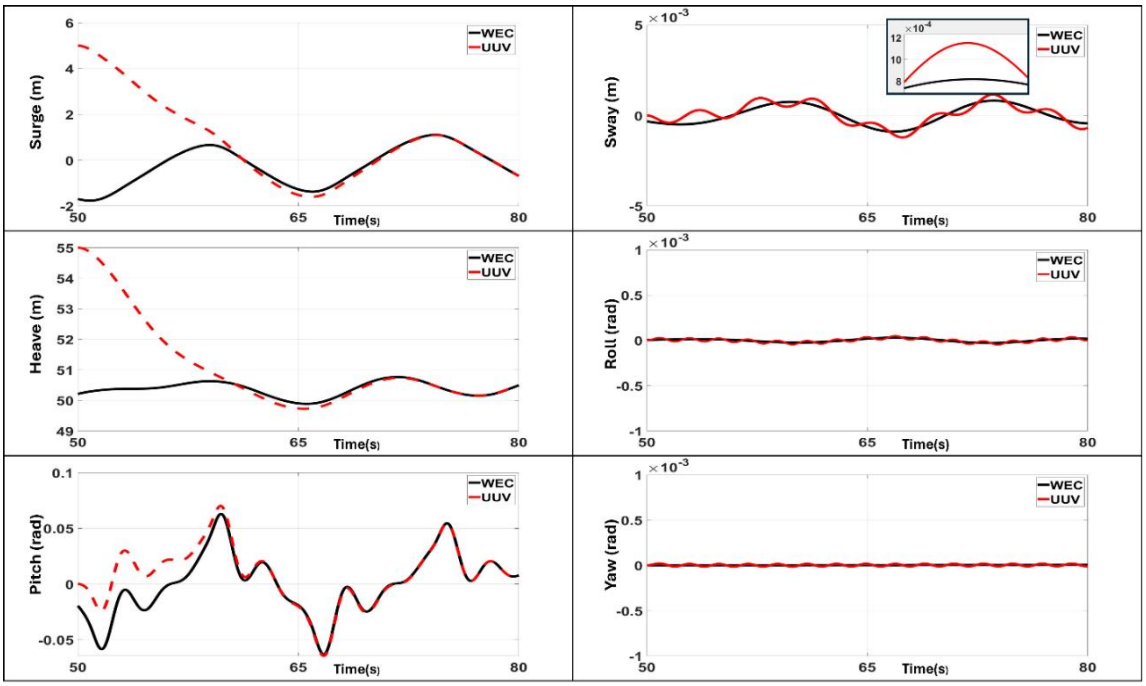

Figure 12: Positional Displacement of UUV and WEC in Actual Scenario with Robust LQR Controller

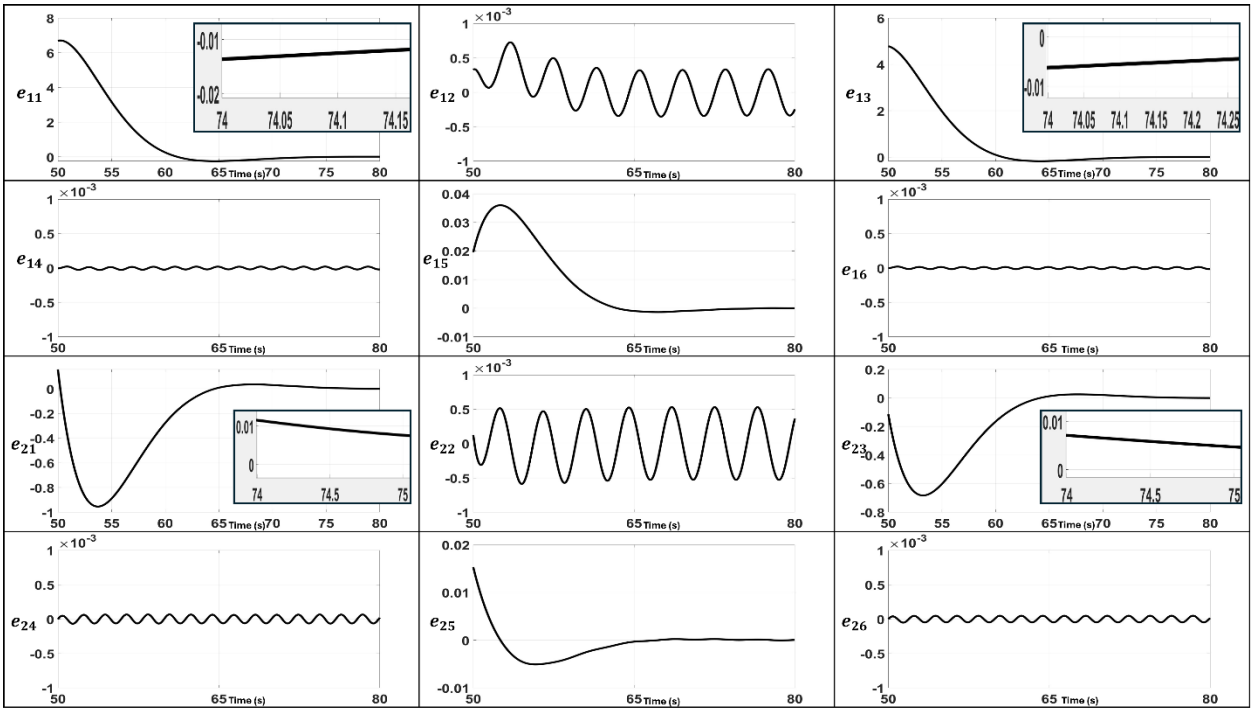

Figure 13: Tracking Error States for Actual Scenario using Robust LQR Controller.

Fig. 12 shows the tracking performance of the ROC in the presence of uncertainties. The effort of the SMC control part is specified as: $\gamma = \text{diag}([1,1,1,50,50,50])$, the smoothing factor is selected as: $\alpha = 100$, and the weight matrix $\boldsymbol{G} = [\text{diag}([1,1.5,10,1,1,1])\ \boldsymbol{I}^{6\times 6}\ ]$. The uncertainties are represented similarly to the previous scenario. We can see that using the ROC, the UUV can successfully track the docking trajectories in the presence of uncertainties, and all the tracking error states (in terms of both the position and velocity) can converge to zero in a finite time in contrast to the last case (as presented in Fig. 13). The docking time is observed to be 24.02s, which is slightly more than the ideal system by 0.04s. This shows that the addition of the SMC controller can mitigate the uncertainties caused by the

unmodeled dynamics and external disturbances and drive the actual system to follow the nominal one (which is optimized by the same LQR control component such that the docking time is similar to the ideal case presented first). This can be further evidenced by the convergence of the sliding surface presented in Fig. 14. In the proposed MIMO system, the sliding surface is a vector with six elements. Here, we present only one element since all elements have similar convergence performance. Fig 15 shows actuation signals from the ROC controller for all the six thrusters. The total energy consumed by the UUV to dock is 648.84 Joules, slightly less than the ideal case by 1.26 Joules. Finally, Fig. 16 shows the path of the trajectory followed by the UUV to dock.

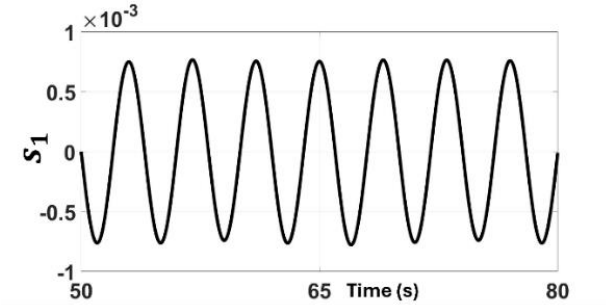

Figure 14: Convergence of Sliding Surface

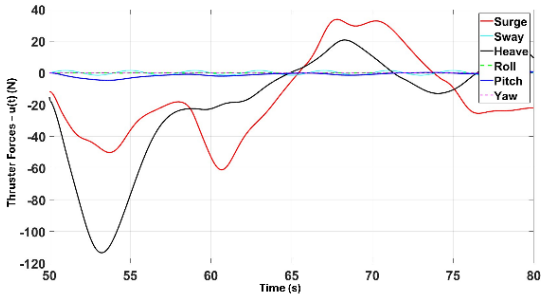

Figure 15: Thruster force for Robust Optimal Controller.

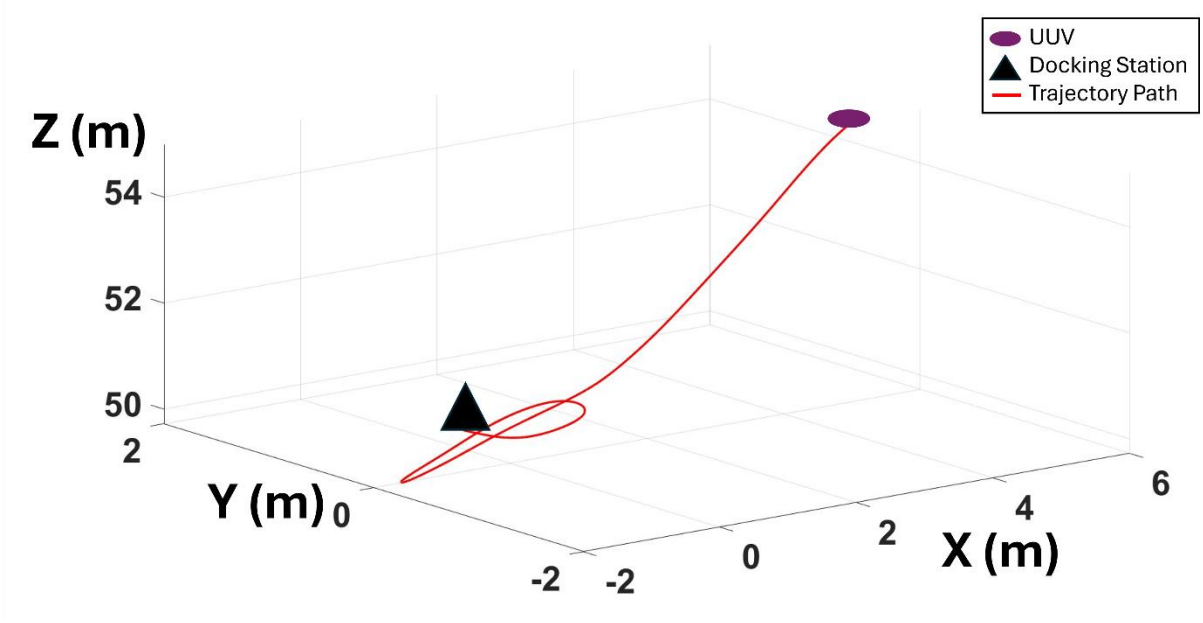

Figure 16: Docking Trajectory of the UUV under uncertainties using ROC

5. Conclusion

In this research we have developed a detailed simulation framework that integrates the WEC, docking station, and UUV accounting for the hydrodynamics of each of this body considering their weight, buoyancy and quadratic drag. The simulation framework can simulate the UUV docking and charging performance efficiently and accurately. The simulation framework is evaluated with different wave conditions to accurately track the hydrodynamics of the integrated WEC and suspended docking station below. Using the simulation framework, we have developed a Robust Optimal Controller to optimize the UUV docking performance subject to dynamic ocean environments and uncertainties. The simulation framework developed for this study not only facilitated precise experiments but also laid a foundational platform for future research in this domain.

The study has successfully demonstrated the efficacy of the ROC in its ability to manage the complex dynamics between a UUV and WEC for docking. In a real-world scenario, the uncertainties caused by unmodelled dynamics of the WEC and UUV along with external disturbances needs to be accounted for as they significantly affect the relative UUV tracking towards the docking stations placed beneath the WEC. The integration of the SMC controller with

LQR was able to significantly mitigate the uncertainties present in a real-world scenario and drive the system towards following the nominal dynamics. The ROC was able to achieve a docking time of 42.16s with uncertainties present and on-par with the ideal system's docking time.

In the future, we plan to account for the tether forces acting on the UUV and the ocean currents acting on both the UUV and WEC, which will realize a system for practical deployment in ocean-based research. We also plan to improve the control design such that the control can explicitly incorporate hard constraints (e.g., the thrust force limitations). Moreover, in this study, we have demonstrated the feasibility of significantly improving the UUV's autonomy for varied ocean missions. In future work, we will also leverage the developed autonomous platform for offshore structure health monitoring and fault diagnosis (e.g., mooring systems of WECs and Floating Offshore Wind Turbines [28]) by further developing computer vision and machine learning techniques.

Acknowledgement

This research is supported in part by NSF under grant CMMI – 2138522.

References

[1] Macreadie, Peter I., et al. "Eyes in the sea: unlocking the mysteries of the ocean using industrial, remotely operated vehicles (ROVs)." *Science of the Total Environment* 634 (2018): 1077-1091.

[2] McLean, Dianne L., et al. "Enhancing the scientific value of industry remotely operated vehicles (ROVs) in our oceans." *Frontiers in Marine Science* 7 (2020): 220.

[3] Bae, I. and Hong, J., 2023. Survey on the developments of unmanned marine vehicles: intelligence and cooperation. *Sensors*, *23*(10), p.4643.

[4] Ewachiw Jr, Mark Alexander. *Design of an autonomous underwater vehicle (auv) charging system for underway, underwater recharging*. Diss. Massachusetts Institute of Technology, 2014.

[5] Drew, Benjamin, Andrew R. Plummer, and M. Necip Sahinkaya. "A review of wave energy converter technology." (2009): 887-902.

[6] Hamilton, A. "Wave-Energy Conversion for Oceanographic Applications." *Proceedings of the 2017 1st Marine Energy Technology, Washington, DC* (2017).

[7] Copping, Andrea, et al. "Maritime renewable energy markets: power from the sea." *Marine Technology Society Journal* 52.5 (2018): 99-109.

[8] Townsend, Nicholas, and Ajit Shenoi. "Recharging autonomous underwater vehicles from ambient wave induced motions." *2013 OCEANS-San Diego*. IEEE, 2013.

[9] Wallen, Jonathan, Nicholas Ulm, and Zhuoyuan Song. "Underwater docking system for a wave energy converter based mobile station." *OCEANS 2019 MTS/IEEE SEATTLE*. IEEE, 2019.

[10] Windt, Christian, Josh Davidson, and John V. Ringwood. "High-fidelity numerical modelling of ocean wave energy systems: A review of computational fluid dynamics-based numerical wave tanks." *Renewable and Sustainable Energy Reviews* 93 (2018): 610-630.

[11] Bacelli, Giorgio, and John V. Ringwood. "Numerical optimal control of wave energy converters." *IEEE Transactions on Sustainable Energy* 6.2 (2014): 294-302.

[12] Zou, Shangyan, et al. "Optimal control of wave energy converters." *Renewable energy* 103 (2017): 217-225.

[13] Davidson, Josh, Simone Giorgi, and John V. Ringwood. "Linear parametric hydrodynamic models for ocean wave energy converters identified from numerical wave tank experiments." *Ocean Engineering* 103 (2015): 31-39.

[14] Chen, Ming, et al. "A unified simulation framework for wave energy powered underwater vehicle docking and charging." *Applied Energy* 361 (2024): 122877.

[15] Xuhui, Yue, et al. "A novel nonlinear state space model for the hydraulic power take-off of a wave energy converter." *Energy* 180 (2019): 465-479.

[16] von Benzon, Malte, et al. "An open-source benchmark simulator: Control of a blueUUV2 underwater robot." *Journal of Marine Science and Engineering* 10.12 (2022): 1898.

[17] Sans-Muntadas, Albert, et al. "A hybrid approach to underwater docking of AUVs with cross-current." *OCEANS 2016 MTS/IEEE Monterey*. IEEE, 2016.

[18] Vivekanandan, Rakesh, Dongsik Chang, and Geoffrey A. Hollinger. "Model predictive control for underwater vehicle rendezvous and docking with a wave energy converter." *Proc. IEEE International Conf. on Robotics and Automation Workshop on Reliable AI for Marine Robotics: Challenges and Opportunities, virtual*. 2021

[19] Vivekanandan, Rakesh, Dongsik Chang, and Geoffrey A. Hollinger. "Autonomous underwater docking using flow state estimation and model predictive control." *2023 IEEE International Conference on Robotics and Automation (ICRA)*. IEEE, 2023.

[20] Cummins, W. E. "The impulse response function and ship motion." *Report 1661, Department of the Navy, David W. Taylor Model Basin, Hydromechanics Laboratory, Research and Development Report, October 1962* (1962).

[21] Raghavan, V., et al. "A comparative study on BEM solvers for Wave Energy Converters." *Trends in Renewable Energies Offshore* (2022): 441-447.

[22] Yu, Yi-Hsiang, et al. *Experimental wave tank test for reference model 3 floating-point absorber wave energy converter project*. No. NREL/TP-5000-62951. National Renewable Energy Lab.(NREL), Golden, CO (United States), 2015.

[23] Bonfanti, Mauro, et al. "On Optimal Control for Nonlinear Hydraulic PTO in Wave Energy Conversion." *2023 3rd International Conference on Electrical, Computer, Communications and Mechatronics Engineering (ICECCME)*. IEEE, 2023.

[24] Zou, Shangyan, and Ossama Abdelkhalik. "Control of wave energy converters with discrete displacement hydraulic power take-off units." *Journal of Marine Science and Engineering* 6.2 (2018): 31.

[25] Zhou, X., Zou, S., Weaver, W.W. and Abdelkhalik, O., 2022. Assessment of electrical power generation of wave energy converters with wave-to-wire modeling. *IEEE Transactions on Sustainable Energy*, *13*(3), pp.1654-1665.

[26] Pang, Hai-Ping, and Qing Yang. "Robust LQR tracking control for a class of affine nonlinear uncertain systems." *2012 24th Chinese Control and Decision Conference (CCDC)*. IEEE, 2012.

[27] Zou, Shangyan, et al. "Wave energy converter arrays: A methodology to assess performance considering the disturbed wave field." *Renewable Energy* (2024): 120719.

[28] Liu, Yixuan, et al. "Physics-guided data-driven failure identification of underwater mooring systems in offshore infrastructures." *Health Monitoring of Structural and Biological Systems XVIII*. Vol. 12951. SPIE, 2024.